

Butt-joint regrowth method by MOCVD for integration of evanescent wave coupled photodetector and multi-quantum well semiconductor optical amplifier

Feng Xiao(肖峰), Qin Han(韩勤), Han Ye(叶焓), Shuai Wang(王帅), Zi-Qing Lu(陆子晴), and Fan Xiao(肖帆)
Citation: Chin. Phys. B, 2022, 31 (**4**): 048101. DOI: 10.1088/1674-1056/ac272b
Journal homepage: http://cpb.iphy.ac.cn; http://iopscience.iop.org/cpb

What follows is a list of articles you may be interested in

Characterization of the N-polar GaN film grown on C-plane sapphire and misoriented C-plane sapphire substrates by MOCVD

Xiaotao Hu(胡小涛), Yimeng Song(宋祎萌), Zhaole Su(苏兆乐), Haiqiang Jia(贾海强), Wenxin Wang(王文新), Yang Jiang(江洋), Yangfeng Li(李阳锋), and Hong Chen(陈弘)
Chin. Phys. B, 2022, 31 (**3**): 038103. DOI: 10.1088/1674-1056/ac3bad

Plasma assisted molecular beam epitaxial growth of GaN with low growth rates and their properties

Zhen-Hua Li(李振华), Peng-Fei Shao(邵鹏飞), Gen-Jun Shi(施根俊), Yao-Zheng Wu(吴耀政), Zheng-Peng Wang(汪正鹏), Si-Qi Li(李思琦), Dong-Qi Zhang(张东祺), Tao Tao(陶涛), Qing-Jun Xu(徐庆君), Zi-Li Xie(谢自力), Jian-Dong Ye(叶建东), Dun-Jun Chen(陈敦军), Bin Liu(刘斌), Ke Wang(王科), You-Dou Zheng(郑有炓), and Rong Zhang(张荣)
Chin. Phys. B, 2022, 31 (**1**): 018102. DOI: 10.1088/1674-1056/ac339d

Distribution of donor states on the surfaceof AlGaN/GaN heterostructures

Yue-Bo Liu(柳月波), Hong-Hui Liu(刘红辉), Jun-Yu Shen(沈俊宇), Wan-Qing Yao(姚婉青), Feng-Ge Wang(王风格), Yuan Ren(任远), Min-Jie Zhang(张敏杰), Zhi-Sheng Wu(吴志盛), Yang Liu(刘扬), and Bai-Jun Zhang(张佰君)
Chin. Phys. B, 2021, 30 (**12**): 128102. DOI: 10.1088/1674-1056/ac0792

Degradation and its fast recovery in a-IGZO thin-film transistors under negative gate bias stress

Jianing Guo(郭佳宁), Dongli Zhang(张冬利), Mingxiang Wang(王明湘), and Huaisheng Wang(王槐生)
Chin. Phys. B, 2021, 30 (**11**): 118102. DOI: 10.1088/1674-1056/ac05aa

Vertical GaN Shottky barrier diode with thermally stable TiN anode

Da-Ping Liu(刘大平), Xiao-Bo Li(李小波), Tao-Fei Pu(蒲涛飞), Liu-An Li(李柳暗), Shao-Heng Cheng(成绍恒), and Qi-Liang Wang(王启亮)
Chin. Phys. B, 2021, 30 (**3**): 038101. DOI: 10.1088/1674-1056/abc547

Butt-joint regrowth method by MOCVD for integration of evanescent wave coupled photodetector and multi-quantum well semiconductor optical amplifier

Feng Xiao(肖峰)[1,2], Qin Han(韩勤)[1,2,†], Han Ye(叶焓)[1], Shuai Wang(王帅)[1], Zi-Qing Lu(陆子晴)[1,2], and Fan Xiao(肖帆)[1,2]

[1] *State Key Laboratory of Integrated Optoelectronics, Institute of Semiconductors, Chinese Academy of Sciences, Beijing* 100083, *China*
[2] *College of Materials Science and Opto-Electronic Technology, University of Chinese Academy of Sciences, Beijing* 100049, *China*

(Received 8 June 2021; revised manuscript received 2 September 2021; accepted manuscript online 16 September 2021)

We have realized integration of evanescent wave coupled photodetector (ECPD) and multi-quantum well (MQW) semiconductor optical amplifier (SOA) on MOCVD platform by investigating butt-joint regrowth method of thick InP/InGaAsP waveguides to deep etched SOA mesas. The combination of inductively coupled plasma etching and wet chemical etching technique has been studied to define the final mesa shape before regrowth. By comparing the etching profiles of different non-selective etchants, we have obtained a controllable non-reentrant mesa shape with smooth sidewall by applying one step $2HBr:2H_3PO_4:K_2Cr_2O_7$ wet etching. A high growth temperature of 680 °C is found helpful to enhance planar regrowth. By comparing the growth morphologies and simulating optical transmission along different directions, we determined that waveguides should travel across the regrowth interface along the [110] direction. The relation between growth rate and mask design has been extensively studied and the result can provide an important guidance for future mask design and vertical alignment between the active and passive cores. ECPD-SOA integrated device has been successfully achieved by this method without further regrowth steps and provided a responsivity of 7.8 A/W. The butt-joint interface insertion loss is estimated to be 1.05 dB/interface.

Keywords: butt-joint regrowth, etching profile, non-reentrant mesa, photonic integration

PACS: 81.05.Ea, 81.15.Kk **DOI:** 10.1088/1674-1056/ac272b

1. Introduction

Explosive increase in network traffic in recent years has put forward higher requirements for the existing communication infrastructures. Due to its small footprint, low coupling loss and cost, photonic integrated circuit (PIC) is one of the most important technologies that can satisfy the demand for high communication capacity.[1] PIC on indium phosphide platform[2] has always been the research focus,[3–6] because of its ability of integrating laser and detector on a single chip. For the realization of InP PICs, it is critical to achieve the compatibility of devices with different structures and materials. One way to integrate different materials is to grow materials successively in-plane, which is known as butt-joint regrowth. So far, various kinds of butt-joint integration have been reported, such as InP/InGaAsP waveguide,[7] InGaAsP–InGaAlAs integration[8] and InP/AlGaInAs/InGaAsP all active components.[9] Particularly, the realization of SOA/waveguide butt-joints ensures the integration of SOA and evanescent wave coupled photodetector without further growth steps.[10] However, few details of SOA/waveguide butt-joint regrowth have been reported on MOCVD platform.

In this paper, we report a study of butt-joint regrowth of thick passive waveguide layers to SOA mesas, using low pressure metal–organic chemical vapor-phase deposition. To obtain non-reentrant mesas with smooth sidewalls before regrowth, we have conducted two different nonselective etchants on dry etched mesas and found a simple one-step etching method. The morphologies of mesas after wet chemical etching and regrowth are observed by scanning electron microscopy. By comparing the growth morphology and simulating optical transmission along different directions, we have found that waveguides should travel across regrowth interface along the [110] direction. In addition, the dependence of growth rate enhancement on the mask layout has been studied by varying mask dimension and their spacing. The results offer an important guidance for future mask design and vertical alignment between active and passive cores. Based on our method, integrated ECPD and SOA has been fabricated without further regrowth steps, whose high responsivity and low butt-joint interface insertion loss demonstrate a promising future of this technology.

2. Experiment procedure

2.1. Growth of MQW SOA layer structure

The major procedure of our experiment is shown in Fig. 1. The structure of InGaAsP MQW SOA (Fig. 1(a)) and InP/InGaAsP regrowth (Fig. 1(d)) were carried out on semi-insulating Fe-doped and (001)-oriented InP substrate by

[†]Corresponding author. E-mail: hanqin@semi.ac.cn

© 2022 Chinese Physical Society and IOP Publishing Ltd

using a low pressure MOCVD reactor. The reactor pressure was 50 mbar. The entire SOA epilayers were first grown at the temperature of 650 °C and growth rate of 5 Å/s. Details are presented in Table 1.

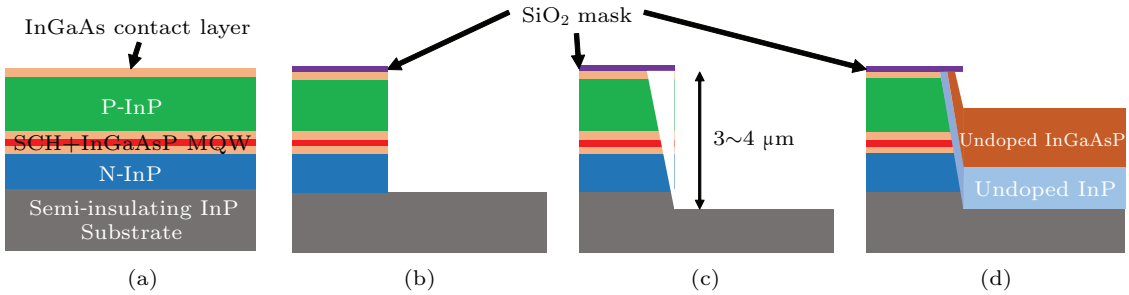


Fig. 1. The procedure of regrowth. (a) Growth of MQW SOA layer structure. (b) Dry etching of SOA. (c) Forming a reentrant mesa shape by wet etching. (d) Regrowth of passive waveguide layers around deep etched mesas.

Table 1. Epitaxial structure of MQW SOA.

Material	Doping (cm^{-3})	Thickness (nm)
P-$In_{0.53}Ga_{0.47}As$	Zn/1.0×10^{19}	100
$In_{0.61}Ga_{0.39}As_{0.85}P_{0.15}$ (Q1.5)	Zn/3.0×10^{18}	25
$In_{0.72}Ga_{0.28}As_{0.61}P_{0.39}$ (Q1.3)	Zn/3.0×10^{18}	25
p-InP	Zn/1.0×10^{18}	1200
p-InP	Zn/1.0×10^{17}	500
$In_{0.72}Ga_{0.28}As_{0.61}P_{0.39}$ (Q1.3)	u.i.d	125
MQW	u.i.d	150–250
$In_{0.72}Ga_{0.28}As_{0.61}P_{0.39}$ (Q1.3)	u.i.d	125
n-InP	Si/2.0×10^{18}	500
$In_{0.88}Ga_{0.12}As_{0.26}P_{0.74}$ (Q1.06)	u.i.d	50
InP	u.i.d	500
InP (001) surface	Semi-insulating	

2.2. Definition of mesa shape

A non-reentrant mesa profile[11] and overhanging SiO_2 masks[12] (as shown in Fig. 1(c)) before regrowth are helpful to suppress mask overgrowth and achieve surface planarity. The non-reentrant mesa means that the narrowest portion of the mesa is at the top in contact with the mask. The mask overhang over this kind of mesa forms a sharp corner at the top of the mesa, screens the mesa top from the ambient and limits the concentration of reactants available for growth. The growth rate is then significantly reduced at the mesa top so that the top end of the growing layer from the mesa sidewall remains under the mask until the growth on the base plane is planarized, preventing the occurrence of mask overgrowth. To obtain a non-reentrant mesa with mask overhang, pure non-selective wet etching was the most common method.[11–16] However, due to the nature of diffusion-limited reaction during the etching,[17] supply of etchants is more abundant near mask edge. Sunken grooves are usually produced around the mask edges. Regrown waveguide layers on this kind of profiles are not flat enough to obtain practical optical coupling efficiency, and thus preclude the implement of integration of passive waveguides and laser structures. In this study, a two-step etching method, i.e., a combination of III–V inductively coupled plasma etching and wet chemical etching is employed.

As shown in Fig. 1(b), a 500–600 nm thick SiO_2 was deposited by using plasma enhanced chemical vapor deposition (PECVD) and patterned by means of conventional photolithography. In order to remove the entire SOA epitaxial layers outside masked areas, we have firstly employed Cl_2/Ar/CH_4 III–V inductively coupled plasma etching (Fig. 1(b)) and after that, a wet chemical etching (Fig. 1(c)). Figure 2 shows the etched profiles after ICP etching. The profiles along [110] and [1$\bar{1}$0] are almost identical due to the anisotropy of ICP etching. Details of wet etchants we used in this study are listed in Table 2.

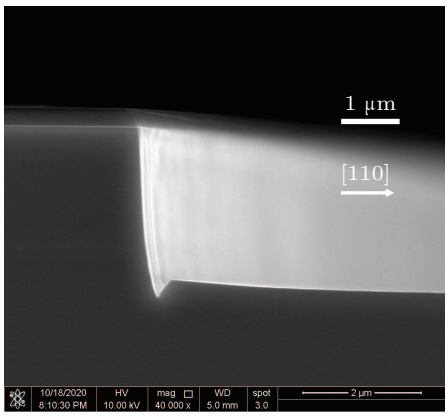


Fig. 2. Etched profile of SOA mesas by ICP etching.

Table 2. Etchants used to define mesa shape.

Solution	Composition	Selective or non-selective
Solution A Br:HBr:H_2O	1:25:106	Nonselective
Solution B HBr:H_3PO_4: $K_2Cr_2O_7$ (saturated in water)	2:2:1	Nonselective

Solutions A and B are all HBr-based non-selective etchants. All etchings are carried out at the temperature of 0 °C without stirring and under ambient illumination.

2.3. Regrowth of passive waveguide layers around deep etched mesas

After etching all the unprotected epi-layer down to the substrate, the wafer was rinsed in oxygen plasma and

etched in concentrated H_2SO_4 for 2 min to remove any organic contamination, surface damage and native oxide layer. Finally, one undoped InP layer and one undoped waveguide core layer $In_{0.88}Ga_{0.12}As_{0.26}P_{0.74}$ were regrown. The $In_{0.88}Ga_{0.12}As_{0.26}P_{0.74}$ layer was lattice-matched material with a bandgap of 1.06 μm.

3. Result and discussion

3.1. Choice of non-selective etchants

In this study, the ICP etching went through the entire laser epi-layers and stopped in the semi-insulating substrate. The mesa after ICP etching is 2.7–2.8 μm high. Then the wafer went through a one-step non-selective etching. Figure 3 shows the etched profiles of non-selective etchants A and B.

Results of non-selective etching As can be seen from Fig. 3, etched profiles on mesas differ dramatically from those on (001) flat surfaces without mesa. The etch rate at the top of mesa is quite higher than that at the bottom of the mesa. For example, in Fig. 3(c), the lateral etch depth, i.e., the mask overhang at the top of mesa is 900 nm, while the etch depth at the bottom of mesa is 300 nm. This phenomenon has also been studied by Fang *et al.*[18] All mesas along both directions exhibit non-reentrant profiles. In addition, the surface near mesa sidewall is groove-free and connects to the sidewall through a very small inclined angle.

The etching profiles along the $[1\bar{1}0]$ and [110] directions are different. Along the [110] direction, the sidewall profile exhibits crystal behaviors. However, as for the $[1\bar{1}0]$ direction, round corners are main characteristics.

Etchant B is more suitable than etchant A to obtain a smooth sidewall profile. When etch time is short (30 s), there is a bump of p-InP on the sidewall along [110] for the case of etchant A (Fig. 3(a)). The bump is even shaper and bigger along the $[1\bar{1}0]$ direction (Fig. 3(e)). The bump may affect the material quality of regrowth[19] and even cause optical absorption. Interestingly, it is found that the bump seems to disappear after longer etch time, as can be seen in Figs. 3(b) and 3(f). This phenomenon has not been reported by other researchers before. However, when using etchant B, the sidewall profile is quite smooth along both crystal directions, even at a short etching time (see Figs. 3(e) and 3(g)).

Discussion The non-selective scheme after dry-etching is extremely helpful in obtaining non-reentrant mesa configuration. This non-reentrant profile differs from that by pure non-selective etching. The nearly flat surface near sidewall makes it highly feasible to regrow flat waveguide layers and develop novel butt-joint integration process. The bump occurred on sidewall may be caused by unequal etching rate of different materials on the sidewall surface. As a result, the choice of etchant is essential in one-step non-selective etching. The shrinking of InP bump after long etching time may be explained by diffusion and supply of reactants. The bump is closer to the mask edge when mask overhang becomes large. It takes shorter time for reactants to diffuse to the top of mesa than to bump portion. On the other hand, due to the blocking effect of mask, supply of etchants to the top of mesa is much reduced. Consequently, the concentration of reactants near the top of mesa is much lower than that near bump area. Etching rate near top of mesa drops down and the bump disappears gradually. Although a long etching time can help to smoothen the sidewall, the drawback is that thicker InP will be regrown under waveguide core layer to assure alignment with the MQW region. Thicker InP means longer regrowth time, which will accelerate the inter-diffusion and intermixing of dopants, especially in MQW layer. Those effects may deteriorate the performance of device. In short, the morphology produced by etchant B is smoother and its mesa height is lower. Therefore, etchant B, BPK-221 system is the best etchant we could find to date.

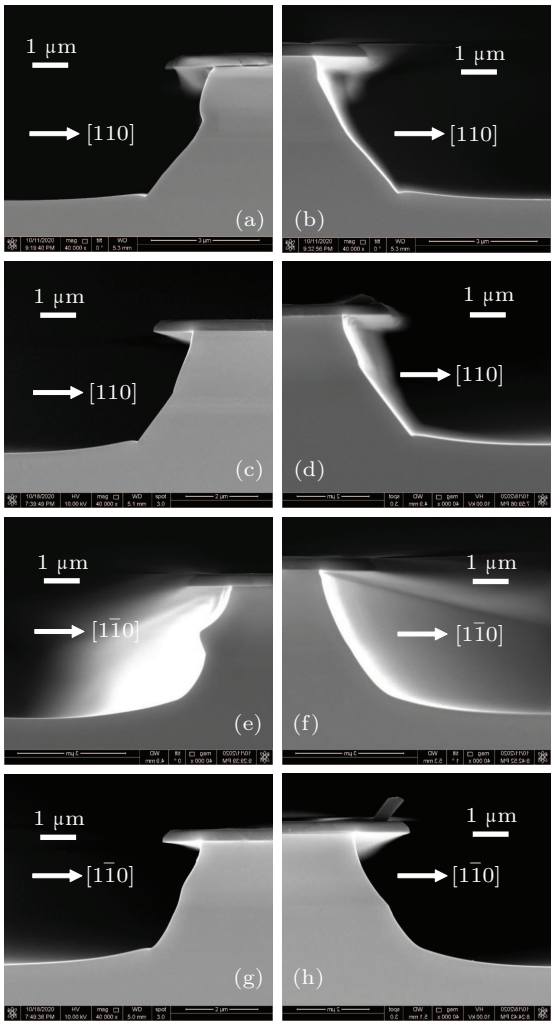


Fig. 3. Etched profiles of ICP etched mesa using etchant A and B. (a) 30 s in A along [110]; (b) 60 s in A along [110]; (c) 30 s in B along [110]; (d) 60 s in B along [110]; (e) 30 s in A along $[1\bar{1}0]$; (f) 60 s in A along $[1\bar{1}0]$; (g) 30 s in B along $[1\bar{1}0]$; (h) 60 s in B along $[1\bar{1}0]$.

3.2. Regrowth profiles

Figure 4 shows the profiles after regrowth along the [1$\bar{1}$0] (a) and [110] (b) directions. In order to increase the diffusion length of reactants, a high growth temperature of 680 °C was used. The reactor pressure was 50 mbar and growth rates for InP and Q1.06 were both 5 Å/s. The growth thickness for InP and Q1.06 were 900 nm and 1000 nm, respectively. The SiO_2 masks were rectangle stripes.

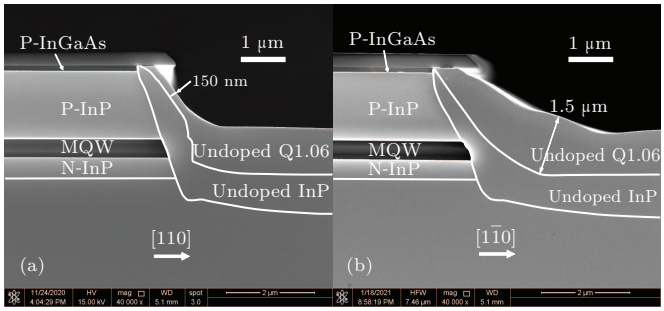


Fig. 4. Growth profiles along [110] (a) and [1$\bar{1}$0] (b) directions. The growth temperature is 680 °C. To delineate boundaries between different layers, samples are stained in $3H_2SO_4$:H_2O_2:$10H_2O$ solution for 20 s. The white lines are added according to the etching boundaries.

Results of regrowth Along the [1$\bar{1}$0] direction, the thickness of regrown InP decreases slowly on the gently sloping surface towards the active region. This spatial variation of thickness forms a horizontal and flat surface for Q1.06 layer to be regrown. At the mesa sidewall, the growth thickness of InP and Q1.06 is much reduced with respect to that on the (001) surface. Especially for the Q1.06 layer, the ratio of growth rate on the sidewall to growth rate on (001) surface is about 0.15 μm/1 μm = 0.15. The thickness of InP near MQW region is about 600 nm. This thin layer ensures a negligible expansion of optical field between active and passive waveguide core, thus, a low coupling loss at the butt-joint interface.

Unlike the [110] direction, growth rate on slope surface, i.e., high index surface, seems to be enhanced along the [1$\bar{1}$0] direction. After the growth of InP, the slope of mesa sidewall becomes longer and gentler. As for the Q1.06 near mask edge, its surface is corrugated. Also the thickness on the sidewall can reach 1.5 μm, which is much enhanced than that (1 μm) far away from mask.

Discussion The different growth morphologies along the [110] and [1$\bar{1}$0] directions are the result of the different bonding configurations existing on the planes exposed for growth.[20] It is believed that high temperature enhances both surface migration and desorption.[21] The pronounced slower growth rate at sidewall along the [110] direction is likely due to the enhanced P evaporation from the surface. In order to figure out whether the [110] or [1$\bar{1}$0] direction is suitable for optical transmission, electrical field distribution and butt-joint efficiency based on real growth morphologies are calculated by using 2D-FDTD method. During the calculation, refractive indices are defined at 1550 nm. A light source of fundamental mode of TE polarization is illuminated at the SOA. The butt-joint efficiency is defined as the ratio of the power collected by passive waveguide fundamental mode to the power of light source. Material in the multi-quantum well region was replaced with Q1.3 to prevent light absorption. Figure 5 shows the calculation results. As can be seen from the figure, when light is transmitted along the direction [110], the distribution of optical field is relatively concentrated in the waveguide core. However, when transmitting along the direction [1-10], the optical field expands greatly after passing through regrowth interface, which is caused by the uneven thickness distribution of Q1.06 core layer. In addition, butt-joint efficiency along the [110] direction (0.87) is higher than that along the [1-10] direction (0.72). Therefore, in subsequent integrated devices, waveguides should be fabricated along the [110] direction.

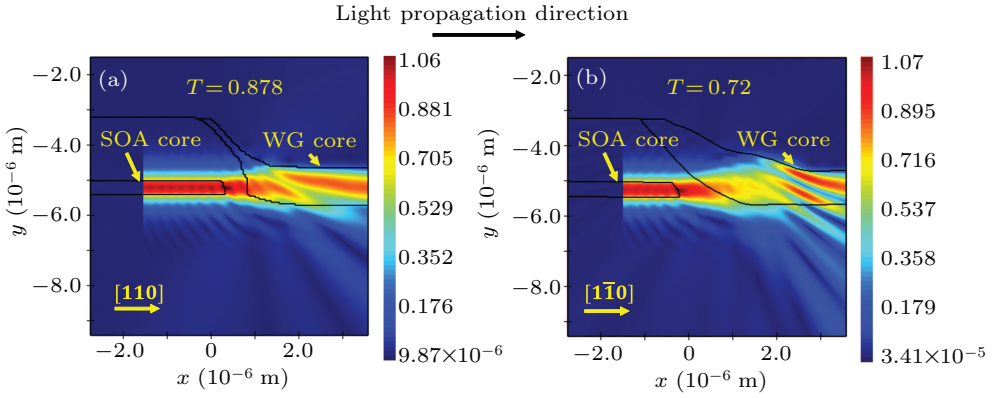


Fig. 5. Simulated electrical field profile and butt-joint efficiency based on real growth morphologies along (a) [110] and (b) [1$\bar{1}$0] directions. The wavelength and polarization of the light source are 1550 nm and TE respectively. 'T' in the picture means the butt-joint efficiency.

3.3. The influence of mask layout on growth rate

Since the thickness of regrown layers near mask edge affects the vertical alignment of waveguides, i.e., the coupling efficiency dramatically, it is essential to know how and how much the thickness is affected by the mask design. To examine the influence of mask layout on growth rate along the

[110] direction, four samples with different mask designs were grown in the same run with a growth rate of 5 Å/s and a growth temperature of 680 °C. Before regrowth, all the samples were etched in BPK-221 solution for 50 s and had mask overhang of 0.8–1.0 μm. The mask of active region is rectangular shape and the details are listed in Fig. 6 and Table 3. All parameters but one in each sample are kept constant. The long edge was aligned with the [110] direction, along which the waveguide will travel across the regrowth interface. After regrowth, each sample was cleaved along the [110] direction as show in Fig. 6. Then thickness of regrown InP and Q1.06 layer was measured at the point 3 μm away from mask edge (Fig. 7(a)) by using the scanning electron microscope. Regrown thicknesses measured on an unmasked substrate are shown in Fig. 7(b). The measured growth thicknesses on the four samples are presented in Fig. 7.

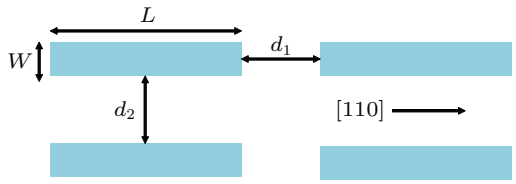


Fig. 6. Four design parameters of mask for regrowth. Four parameters are W (width), L (length), d_1 (longitudinal spacing) and d_2 (transverse spacing).

Table 3. Details of mask design of 4 samples.

Sample	W (μm)	L (μm)	d_1 (μm)	d_2 (μm)
1#	100	300	50, 100, 200, 300, 400	500
2#	80	300	500	100, 200, 300, 400, 500
3#	40, 60, 80, 100, 120	300	500	500
4#	100	200, 300, 400, 500, 600	500	500

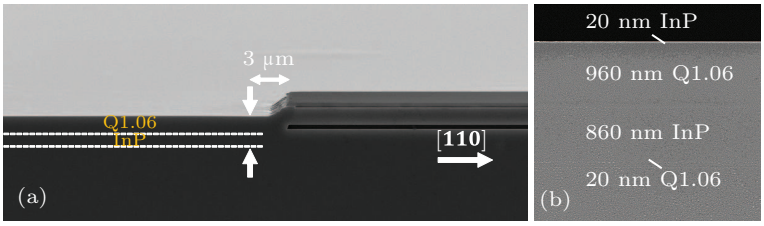


Fig. 7. Position (a) where thickness measurements were performed and regrown thicknesses (b) measured on an unmasked substrate.

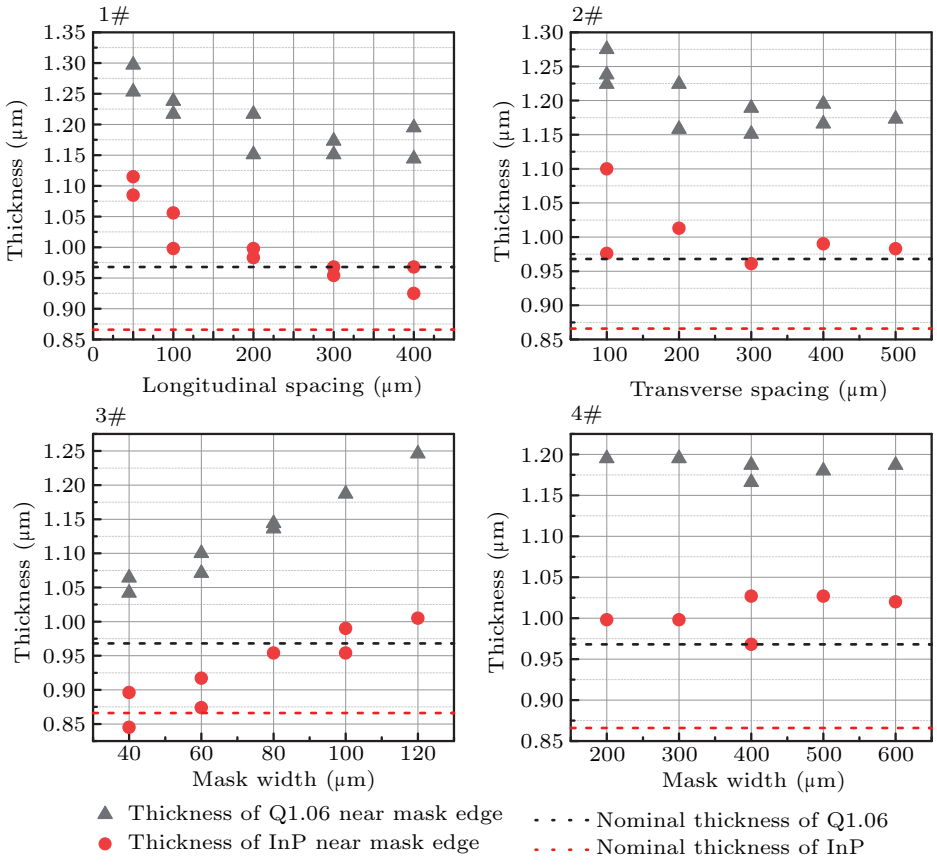


Fig. 8. The growth thickness on the four samples.

The growth rate of Q1.06 layer is more enhanced near mask edge than InP material. Here, we define the growth rate enhancement factor[22] (GRE) as the ratio of the thickness of the selectively grown layer measured 3 μm away from mask edge and the layer thickness in unperturbated area (nominal thickness in Fig. 8). For the case of sample 3, when the mask width is 120 μm, GRE of Q1.06 is $1.25/096 = 1.30$, while GRE of InP is $1.0/0.86 = 1.16$.

The regrowth thickness of Q1.06 and InP layer decreases exponentially with longitudinal and transverse spacing of masks. For the case of sample 1, the thickness of Q1.06 layer dropped from 1.27 μm to 1.18 μm, i.e., a decrease of 90 nm, when longitudinal spacing was increased from 50 μm to 200 μm. However, when longitudinal spacing increased from 300 μm to 400 μm, the thickness of Q1.06 was kept around 1.16 μm. Same tendency can be found for InP layer and in sample 2.

The mask width affects the thickness of selectively regrown layers in a linear way, while the mask length seems not to be the deal. For the case of sample 3, the growth thickness of Q1.06 has gained an incremental of 100 nm once mask width was increased by 40 μm. As for InP layer, the slope of the relation is 75 nm/40 μm. For the case of sample 4, the growth thickness of Q1.06 has stayed within the rage of 1.18 and 1.20, no matter how long mask length is used. Same tendency can be found for the InP layer.

Discussion The lateral vapor phase diffusion from regions above masks can account for the enhanced growth rate near mask edge for selective area growth. The more enhanced growth rate for Q1.06 than InP may be caused by higher diffusion coefficient of Indium decomposed fragments than gallium decomposed fragments. Thus, more gallium than indium species can be absorbed in region close to masks, increasing the growth rate of Ga-containing material near mask edge. The above results with respect to mask dimensions show that our regrowth process is very useful for monolithic integration of active and passive waveguides. The exponentially decreasing regrown thickness suggests that thickness sensitive devices can work as predicted if they are arranged far enough to the masked active region. The nearly independence of growth thickness on mask length enables a free design of SOA device length without degrading coupling efficiency at regrown interface.

3.4. Device fabrication results

After obtaining controllable butt-joint regrowth on the patterned SOA wafer, regrowth of whole evanescent wave coupled photodetector (ECPD) layer structure around SOA mesa was carried out, by using the same etching method and growth conditions as described in previous sections. In addition to InP/InGaAsP waveguide, the ECPD also includes photodetector (PD) layers, which consist of N-InGaAsP contact layer, i-InGaAs absorbing layer, p-InGaAsP upper cladding layer and P-InGaAs contact layer. Figure 9(a) shows the SEM graph of regrowth profile around butt-joint interface by using a 100 μm wide mask. The growth morphology of InP/InGaAsP passive waveguide agrees well with the previous experiment. Although the epitaxial layer of PD has risen above the upper surface of the mask, it does not extend above the mask and exhibits the characteristic of {111} crystal plane at the mask boundary.

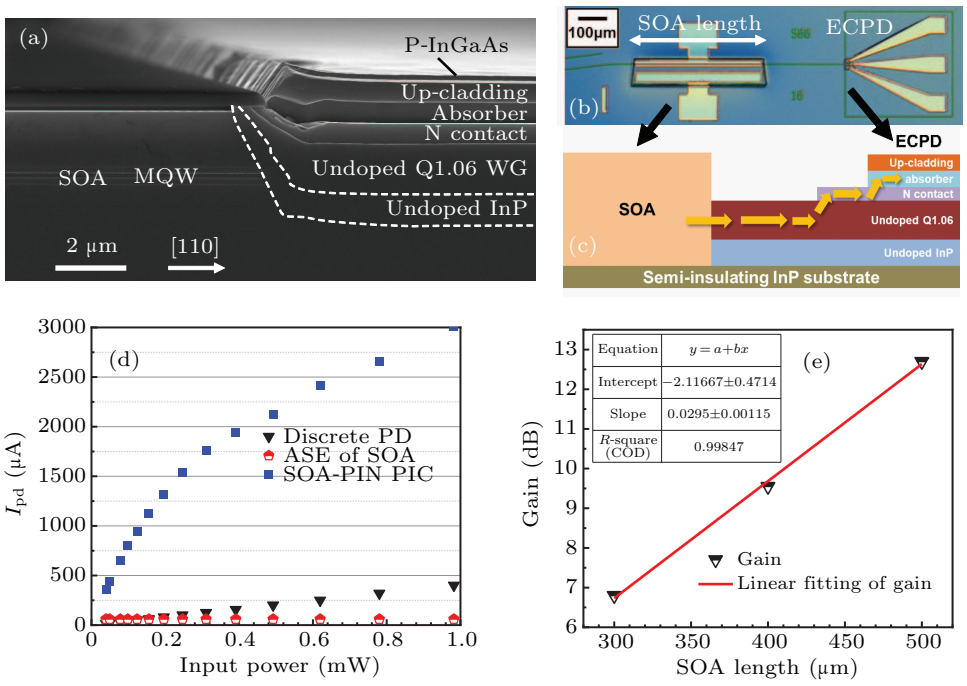


Fig. 9. Fabrication results of integrated SOA and ECPD: (a) Regrowth morphology of InP/InGaAsP waveguide and photodetector around butt-joint interface. (b) Photograph of a fabricated SOA-ECPD chip. The SOA is a 2×500 μm^2 device and the PD size is 5×10 μm^2. (c) Schematic of ECPD corss section. (d) Photocurrent measurement results at 1545 nm under different input power using a tapered single mode fiber. The injection current density for SOA is 9 kA/cm^2. PD is biased at −3 V. (e) Small signal gain versus SOA length and its linear fitting. The injection current density for SOAs is 9 kA/cm^2.

Conventional lithography, dry etching and wet etching processes were then used for the fabrication of SOA-ECPD integrated devices. SiO_2 and photoresist were served as etching mask. SOA and PD are 2×500 μm^2 and 5×10 μm^2, respectively, and they are connected through a 300 μm long waveguide. The passive waveguide is a 2 μm wide shallow ridge waveguide. Figure 9(b) shows an optical photo of the fabricated device.

For ECPD as shown in Fig. 9(c), the light is coupled evanescently from the single-mode Q1.06 waveguide into a multi-mode waveguide, which is composed of n-contact layer and waveguide layer. This stimulates beat effect between multiple modes and produce periodic oscillations in the direction of propagation. By controlling the extended length of the N contact layer, absorber layer at the front end of the PD mesa can contribute to absorption process, improving the responsivity of the detector without affecting the bandwidth.

Figure 9(d) shows photocurrent measurement results of the SOA-ECPD integrated device versus the discrete ECPD. At 9 kA/cm^2 current density and low input power, the SOA-ECPD PIC has a responsivity of 7.8 A/W, which is 12.7 dB higher than the 0.4 A/W of discrete ECPD. The small signal on-chip gain of SOA versus device length is plotted in Fig. 9(e). By calculating the intercept of linear fitting curve, the insertion loss of butt-joint interface can be estimated as dB/interface Consequently, we believe that the studied butt-joint regrowth method is qualified for the integration of SOA and ECPD.

4. Conclusion

We have studied butt-joint regrowth of thick passive waveguide layers around deep etched entire SOA mesas, by using low pressure metal–organic chemical vapor-phase epitaxy. By comparing the etching profile of different etchants, we have achieved a non-reentrant mesa profile with smooth side wall by combination of ICP etching and 2HBr:2H_3PO_4:$K_2Cr_2O_7$ wet etching. A high growth temperature is used to obtain planar regrowth. By comparing the growth morphology and simulating optical transmission along different directions, higher butt-joint coupling efficiency will be obtained along the [110] direction. The relation between growth rate and mask design has been carefully examined and found to provide important guidance for future mask design and photonic integration process. This technology has been successfully employed to realize the integration of evanescent waveguide photodiode and active gain section in a simple way.

Acknowledgements

Project supported by the National Key R&D Program of China (Grant No. 2020YFB1805701), the National Natural Foundation of China (Grant Nos. 61934003, 61635010, and 61674136), and Beijing Natural Science Foundation, China (Grant No. 4194093).

References

[1] Borsato Cunha M S, Lima E S, Andriolli N, Spadoti D H, Contestabile G and Arismar Cerqueira S Jr. 2021 *IEEE J. Sel. Top. Quantum Electron.* **27** 6100308
[2] Tonning P L and Heck M J R 2020 *J. Lightwave Technol.* **38** 5526
[3] Yagi H, Kaneko T, Kono N, Yoneda Y, Uesaka K, Ekawa M, Takechi M and Shoji H 2018 *IEEE J. Sel. Top. Quantum Electron.* **24** 6100411
[4] Kish F, Lal V, Evans P, Corzine S W, Ziari M, Butrie T, Reffle M, Tsai H, Dentai A, Pleumeekers J, Missey M, Fisher M, Murthy S, Salvatore R, Samra P, Demars S, Kim N, James A, Hosseini A, Studenkov P, *et al.* 2018 *IEEE J. Sel. Top. Quantum Electron.* **24** 6100120
[5] Augustin L M, Santos R, Haan E d, Kleijn S, Thijs P J A, Latkowski S, Zhao D, Yao W, Bolk J, Ambrosius H, Mingaleev S, Richter A, Bakker A and Korthorst T 2018 *IEEE J. Sel. Top. Quantum Electron.* **24** 6100210
[6] Arafin S and Coldren L A 2018 *IEEE J. Sel. Top. Quantum Electron.* **24** 6100612
[7] Barbarin Y, M Bente E A J, de Vries T, den Besten J H, van Veldhoven P J, Sander-Jochem M J H, Smalbrugge E, van Otten F W M, Geluk E J, Heck M J R, Leijtens X J M, van der Tol J G M, Karouta F, Oei Y S, Nötzel R and Smit M K 2005 *Proceedings of the 10th Annual Symposium IEEE/LEOS Benelux,* December 1–2, 2004, Mons, Belgium, p. 89
[8] Kitatani T, Shinoda K, Tsuchiya T, Sato H, Ouchi K, Uchiyama H, Tsuji S and Aoki M 2004 *16th IPRM. 2004 International Conference on Indium Phosphide and Related Materials,* May 31–June 4, 2004, Kagoshima, Japan, p. 480
[9] Kulkova I V, Kadkhodazadeh S, Kuznetsova N, Huck A, Semenova E S and Yvind K 2014 *J. Cryst. Growth* **402** 243
[10] Gibis R, Kizuki H, Albrecht P, Harde P, Urmann G, Kaiser R and Kunzel H 2000 *J. Cryst. Growth* **209** 463
[11] Zilko J L, Segner B P, Chakrabarti U K, Logan R A, Lopata J, Vanharen D L, Long J A and McCrary V R 1991 *J. Cryst. Growth* **109** 264
[12] Nakai K, Sanada T and Yamakoshi S 1988 *J. Cryst. Growth* **93** 248
[13] Huang R T, Jiang C L, Appelbaum A, Renner D and Zehr S W 1990 *J. Electron. Mater.* **19** 1313
[14] Lee B T, Logan R A and Chu S N G 1993 *J. Cryst. Growth* **130** 287
[15] Karlicek R F, Coblentz D L, Logan R A, Hayes T R, Pawelek R and Byrne E K 1993 *J. Cryst. Growth* **131** 204
[16] Cheng L, Fan J, Janssen D, Guo D, Chen X, Towner F J and Choa F S 2012 *J. Electron. Mater.* **41** 506
[17] Notten P H L, Kelly J J and Kuiken H K 1986 *J. Electrochem. Soc.* **133** 1226
[18] Fang R Y, Bertone D, Morello G and Meliga M 1997 *J. Electrochem. Soc.* **144** 3940
[19] Shinoda K, Taike A, Sato H and Uchiyama H 2003 *J. Electrochem. Soc.* **150** G117
[20] Lourdudoss S, Messmer E R, Kjebon O and Landgren G 1995 *J. Cryst. Growth* **152** 105
[21] Nordell N and Borglind J 1992 *Appl. Phys. Lett.* **61** 22
[22] Van Caenegem T, Moerman I and Demeester P 1997 *Prog. Cryst. Growth Charact. Mater.* **35** 263